Speed Measurement Algorithms for Low-Resolution Incremental Encoder Equipped Drives: a Comparative Analysis

Roberto PETRELLA
DIEGM
University of Udine, Faculty of Engineering
Via delle Scienze, 208, I-33100 Udine, Italy
roberto.petrella@uniud.it

Marco TURSINI
DIEI
University of L'Aquila, Faculty of Engineering
Poggio di Roio, I-67040 L'Aquila, Italy
tursini@ing.univaq.it

Luca PERETTI, Mauro ZIGLIOTTO
DTG
University of Padova, Faculty of Engineering
Stradella S. Nicola, 3, I-36100 Vicenza, Italy
luca.peretti@unipd.it, mauro.zigliotto@unipd.it

Abstract - **Precise motion control requires high-accuracy and high-bandwidth feedback speed information, often calculated by direct measurement of the rotor position available through the incremental encoder equipping the drive. The resolution of the encoder heavily affects the cost of the drive and the accuracy and bandwidth of the calculated speed. The limitations introduced by a low resolution encoder can be partially reduced by a proper speed calculation (or estimation) algorithm, that therefore plays a key role in modern drive systems. In this paper a comparative analysis of state-of-art speed measurement and estimation algorithms suitable for low-resolution incremental encoder equipped drives is presented, aiming at highlighting the specific feature of each one, both from the performance point of view, and from the computational requirements needed for actual implementation. The paper proposes itself as a guide for engineers in the complex choice of the best solution for each application.**

Keywords: incremental encoders, speed measurement.

I. INTRODUCTION

Position and rotor speed are required for high performance servo drive systems, where rotary incremental encoder is probably the most frequently adopted position transducer, [1][2][3]. The resolution of the encoder heavily affects the cost of the drive and the accuracy and bandwidth of the calculated speed. A low level information is provided in the form of two pulse trains, that are transmitted to the control system which calculates actual rotor position and speed needed for motor control. Starting from angular displacement, different processing solutions can be employed aimed at speed calculation ([2]÷[8]), whose choice is a function of the accuracy and bandwidth required by the particular application, the processing performance of the adopted microcontroller or programmable logic, system cost and complexity, a strong trade-off commonly existing among those features. The limitations introduced by low-resolution encoders can be partially reduced by the choice of a proper speed calculation (or estimation) algorithm, therefore playing a key role in modern drive systems.

A class of the speed estimation methods are based on the direct measurement of the frequency and/or the period of the quadrature encoder signals, [3][5]÷[9]. In [3] the main aspects and error sources coming from frequency and period measurement are addressed and discussed. Different solutions are given in literature to overcome the limitations of those basic measurement methods by introducing filtering and processing capabilities. In [5] a sort of regressive refinement of the basic measurement is proposed allowing to select the relative accuracy and delay of the estimated average speed information. Some methods are based on an equivalent analogical continuous time transformation of the digital quadrature signals. In [6] square pulses from the encoder are first turned into ramp using analogical electronics and then sampled. Samples are processed by a linear regression algorithm in order to extrapolate backward and determine the starting poing of each pulse very accurately.

Application specific hardware is adopted in [7][8] in order to realise an accurate processing of the encoder signals by means of mixed-mode frequency and period measurement. The problem of the asynchronous relationship between incoming pulses and digital circuitry is addressed and solved by means of dedicated subsystems. A novel mixed time and frequency measurement technique of the encoder signals is proposed in [10] and [11] assuring very high accuracy and bandwidth for the calculated rotor speed. The iterative formulation of the algorithm and the limited hardware requirements allows its implementation by means of a standard μC or by simple dedicated hardware.

More recently the availability of cheap and widespread CMOS techology processes, allows the implementation of dedicated chips including position measurement, speed and acceleration estimation and communication resources, [9]. The idea of embedding processing and communication resources into the same hardware unit allows the development of smart sensors. Incremental position is acquired at the encoder level and rotor speed is calculated by the embedded μC or dedicated chips and transmitted to the remote servo drive as high level information, [11]. Communication between the smart encoder and the servo drive system must satisfy the real-time requirements of the controller and has then to be realised via high speed communication link. The reliability of the exchanged information has to be guaranteed in all the operating conditions, leading to the introduction of fail-proof communication protocol, both at the physical and data link layers.

Several methods have been developed in order to obtain high precision position and speed detection which are commonly addressed as “estimation methods”, [2][4][12][13]. Proper state models of the dynamic behaviour of mechanical

subsystem (including position, speed, acceleration, etc.) are in fact arranged providing speed estimation in real-time based on easily measurable quantities and system parameters by means of state observers and estimators, [2][4].

In [12] an extended Kalman filter is adopted for speed estimation where a non-linear state model is built based on the orthogonal components representation of a rotating space vector, generated from the encoder position. The filter allows to estimate both the components of the vector position (*sin-cos*) and the frequency (ω) with an accuracy which is independent from the transducer's resolution. Moreover one sample of the estimated orthogonal components and the estimated frequency is available at each execution of the EKF, that is roughly 100÷200μs. In [13] a similar approach has been adopted but a linear system is considered, thus allowing the use of stationary Kalman filter and reducing the number of real-time operations to be performed. Moreover the same observer also provides an acceleration estimate.

More recently the combination of accurate speed measurement with low-resolution sensors and *sensor-less* control of drives is becoming more and more attractive as it allows the development of very cheap and reliable drives for the consumer market, [14].

All the observer-based methods share the feature of providing high accuracy of the speed estimation with satisfactory dynamic performance. But they suffer from the dependence on system parameters or design parameters that have to be carefully chosen during system development and tuning, [2][4]. Moreover the obtainable steady-state and transient performance are often a function of the operating conditions, e.g. speed and/or acceleration values. In some cases a design trade-off exists between low steady-state speed estimation errors and high dynamic performance, which could lead to the adoption of complex adaptive observers. Finally, the implementation effort and execution times of those methods could be very high and normally require high performance processing systems.

In this paper a comparative analysis of state-of-art speed measurement and estimation algorithms suitable for low-resolution incremental encoder equipped drives is presented. It aims at highlighting the specific feature of each one, both from the performance point of view, and from the computational requirements needed for actual implementation.

II. FREQUENCY/PERIOD MEASUREMENT

A. Frequency measurement

The classical and probably the simplest method to measure rotor speed is the direct measure of the frequency of the encoder pulses. Typically the number of the observed pulses inside a given and constant-width time-window is counted. Angular speed is then approximated to the discrete incremental ratio, that is constant speed is considered inside the observation windows:

$$\omega = \frac{d\theta}{dt} \cong \frac{\Delta\theta}{T_{sc}} \cong \frac{2\pi \cdot \Delta N}{N_p \cdot T_{sc}} [rad \cdot s^{-1}] \rightarrow \frac{60 \cdot \Delta N}{N_p \cdot T_{sc}} [RPM] \qquad (1)$$

where N_p is the number of pulses per revolution (after quadrature decoding), T_{sc} is the time-window and ΔN is the number of observed pulses inside that window. As a result, one has a quantisation error superimposed to the effective mean speed inside the observation window which depends on the uncertainty on the measured number of pulses ΔN, caused by the lack of synchronisation between encoder pulses and the observation window itself.

The speed measurement quantisation error $\Delta\omega$ is:

$$\Delta\omega = \frac{2\pi}{N_p T_{sc}} [rad \cdot s^{-1}] \rightarrow \frac{60}{N_p T_{sc}} [RPM] \qquad (2)$$

Equation (2) shows that the quantisation error is independent from the operating speed and it depends only on the number of encoder pulses per revolution and the observation time window. Therefore the relative accuracy of the method is a function of the speed itself, as expressed by the following formula:

$$e_\omega\% = \frac{2\pi}{\omega \cdot N_p T_{sc}} \cdot 100 \qquad (3)$$

In Fig. 1 both transient and steady-state operating conditions are simulated with different values of the number of pulses per revolution (N_p) and the observation window (T_{sc}). Actual and measured speed by adopting a pure frequency measurement are shown. In Fig. 1a a longer observation window (400μs) is considered with a low resolution encoder (1000 pulses/revolution), whilst in Fig. 1b a shorter observation

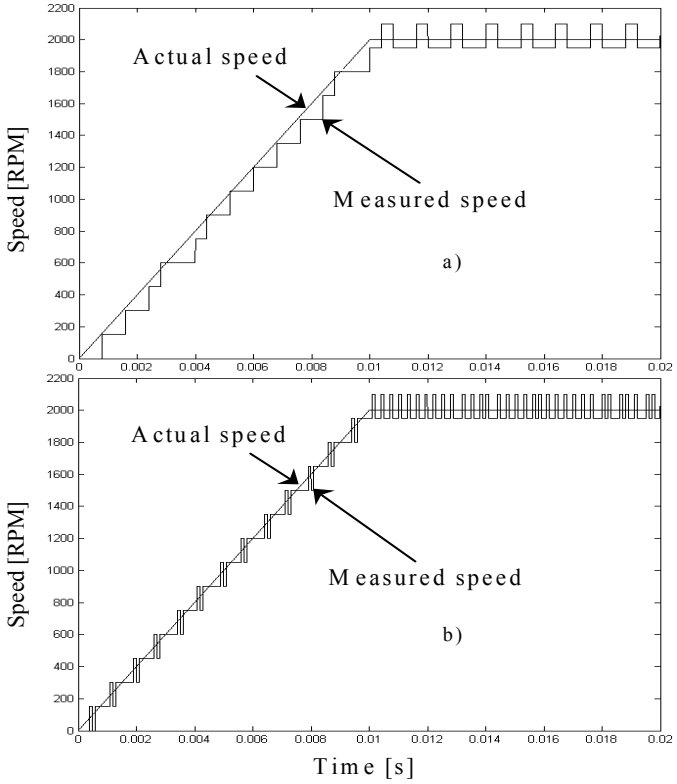

Fig. 1 – Speed quantisation errors by means of pure frequency measurement (simulation results, a) N_p=1000, T_{sc}=400μs; b) N_p=4000, T_{sc}=100μs).

window (100μs) is considered with a higher resolution encoder (4000 pulses/revolution). As the product N_pT_{sc} is constant for both cases, the absolute measurement error is the same and is independent on speed value as shown in (2).

In Fig. 2 the situation is resumed in graphical format for some practical cases. In middle and high speed region the quantisation error causes a percentage error which in many cases is acceptable, but in very low speed region the amplitude of the quantisation error is the same as the effective speed and the percentage error becomes intolerable. Requirements for cost reduction of drive systems suggest the use of low resolution transducers, leading to higher speed measurement errors in the low-speed region and to an intolerable reduction of system performance.

A commonly adopted way to reduce quantisation error, especially in the low speed region, is to increase the speed sampling time and control period, but this solution reduces the bandwidth of the controller. Low-pass filtering can be adopted aiming at reducing steady-state as well as transient error and remove the excess quantisation error, but the additional lag time introduced by the filter degrade the performance of the speed control loop and sometimes is not tolerable. Good results are achieved by employing moving average based filtering. The width of the window buffer has to be chosen considering the required accuracy of steady-state measurement error and the dynamical performance degradation of the drive. Gain of accuracy is therefore proportional to the length of the window buffer used for filtering.

The implementation of the frequency measuring method is very straightforward, as it requires only the computation of ΔN and one multiplication for the constant terms in (1) if the basic measurement is considered. Incremental position measurement is almost always performed by dedicated quadrature decoder hardware, commonly found inside dedicated microcontrollers. The implementation of a n^{th} order filter is very simple in its basic forms, i.e. low-pass low-order, but can become very difficult and time consuming if higher order and fixed-point arithmetic are considered, due to the possible instability introduced by coefficient and multiplication truncation with the chosen numerical representation. On the other hand, the implementation of a moving average filter is very simple from the computational point of view, requiring only the computation of (1) and one sum and one subtraction at each step, but it needs more memory and a proper circular addressing of the window buffer.

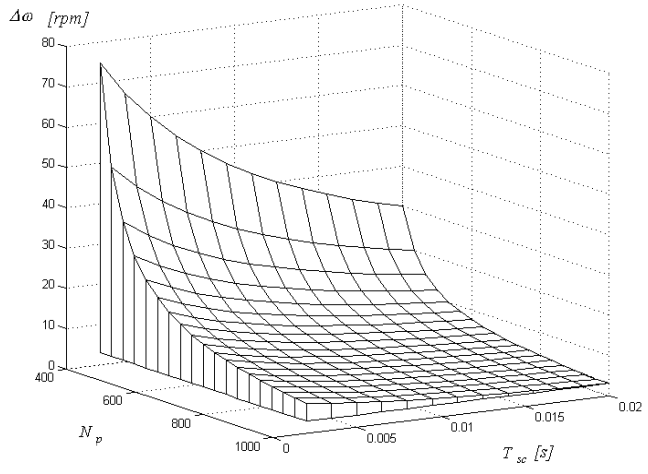

Fig. 2 – Speed quantisation error obtained by means of pure frequency measurement.

B. Period measurement

An alternative solution to the reduction of the measurement error is to switch from frequency to period measurement at a certain level of (low) speed. The measurement is realised by counting the number of periods of a high frequency signal inside one (or more) encoder pulses, Fig. 3. The following formula is obtained under the hypotesis that motor speed is constant and only one period of the encoder signal is considered:

$$\omega = \frac{d\theta}{dt} \cong \frac{\Delta\theta}{n \cdot T_{hf}} \cong \frac{2\pi}{N_p \cdot n \cdot T_{hf}} \; [rad \cdot s^{-1}] \rightarrow \frac{60}{N_p \cdot n \cdot T_{hf}} \; [RPM] \tag{4}$$

A speed sample can be calculated each period of the encoder signals. Speed sampling period is thus a function of motor speed:

$$T_\omega(\omega) = \frac{2\pi}{N_p \cdot \omega} \; [s] \tag{5}$$

The accuracy of the measurement is related to the ratio between the period of the high frequency counter and that of the encoder signals, that is not an integer value as it depends on motor speed. A calculation of absolute and percentage errors is extremely difficult as it involves non-linear rounding functions. A worst-case condition error could be calculated instead by considering the absolute error of one high frequency pulse, leading to a maximum percentage error limiting locus given by the following formula, i.e. roughly linear with speed:

$$e_\omega\% = \frac{T_{hf}}{\frac{2\pi}{N_p \cdot \omega} - T_{hf}} \cdot 100 \cong \frac{\omega \cdot N_p \cdot T_{hf}}{2\pi} \, . \tag{6}$$

At very low speed the number of high frequency pulses can be extremely high and saturation of the digital timer employed for measurement can occur. Also a speed sample is not available each speed control period, needing an adaptation of the control parameters. In that situation, the quadrature decoding of the encoder pulses can be exploited in order to reduce the width of the measuring window by a factor of four

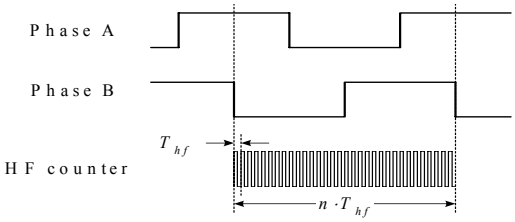

Fig. 3 – Period measurement by high frequency counter.

or a reduction of the frequency of the timer can be considered.

The former solution allows to reduce the speed sampling period and improve the control performance of the drive, but makes the measuring system more sensitive to sensor nonidealities, including variations in the transition locations from their nominal values and phasing errors between encoder channels. When low-cost and low-resolution sensors are employed, nonidealities play the major role in the determination of period measuring errors and has to be carefully analysed in drive design phase. The latter solution needs to switch on-line the frequency of the timer and adapt the coeffients of the equations above.

The implementation of the period measuring method is also straightforward as it requires a simple timer capture unit, commonly found inside recent microcontrollers. Specific hardware subsystems can be considered to overcome digital timer saturation problems (e.g. [7] and [8]) and proper algorithms are needed to filter out the errors introduced by sensor nonidealities, [10][11]. The problem of speed calculation error generated at motor reversion can be easily solved by the identification of motor direction during time measurement and correction of the timer value, [3], but best performance are obtained by means of specific hardware solutions.

III. MIXED MODE FREQUENCY/PERIOD MEASUREMENT

Relative errors given by equations (3) and (6) are plotted as a function of motor speed in Fig. 4 for a common pair of N_p and T_{sc}. Also actual speed errors by period measurement are included. One can notice that period measurement provides higher accuracy at low speed whilest frequency measurement is more accurate at higher speed. There exist a critical speed where the two methods provide the same percentage error, that can be directly calculated by equations (3) and (6):

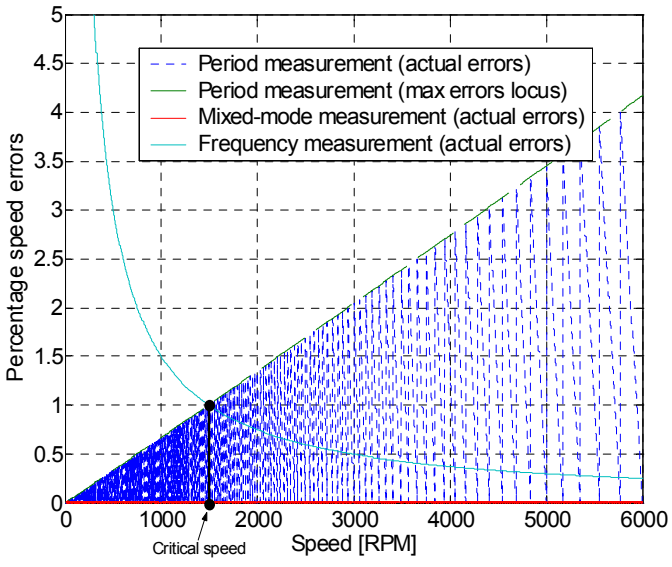

Fig. 4 – Comparison among different measurements methods (N_p=4000, T_{sc}=1ms).

$$\omega_{crit} = \frac{-\pi \cdot T_{hf} + \pi\sqrt{T_{hf}^2 + 4 \cdot T_{hf} \cdot T_{sc}}}{T_{hf} \cdot T_{sc} \cdot N_p} \tag{7}$$

whose value is about 1492 rpm in the considered conditions.

The results of Fig. 4 explain the reason why a mixed-mode frequency and period measurement are normally adopted in industrial drives as a function of motor speed. Lot of papers and patents has been published in the recent past regarding the mixed mode frequency/period measurement, some examples being [3][7][8][9]. The major part of them shares the need of a specific hardware subsystem (e.g. implemented within an FPGA) to accomplish the task of speed estimation, raising the complexity of the drive system. Some solutions are based on a software transition from one method to the other by means of a proper switching function, aiming at providing soft switching with no discontinuities in motor speed calculation. Fig. 4 also shows that both frequency and period measurement assure a relative error that is less than 1% in the considered conditions. The corresponding absolute error can reach the value of 10 rpm, which is not tolerable in lot of high-performance applications.

An interesting approach to mixed-mode frequency and period measurement is presented in [10] and [11], providing extremely low relative errors. The basic idea is to compensate for the quantisation error of pure frequency measurement (2) due to the lack of synchronisation between encoder signals and observation window. This can be done by measuring the time intervals (ΔT_h in Fig. 5) between the bounds of the (basic) observation window (that is T_{sc} in (1)) and incoming encoder pulses. In this way it becomes possible to adapt the window width (T_{eq}) to the nearest integer number of pulses being received, thus zeroing quantisation error. A high accuracy measure of speed within each control cycle (e.g. 100μs) is obtained if one pulse is received at least within it. In case no pulse enters in the basic observation window (low speed operations), an extended observation window is considered made up of an integer number of basic windows and speed information is updated only after the reception of a valid pulse. In this case the width of the extended observation window ($\Sigma T_{sc,acc}$) can be expressed by the sum of each T_{sc}.

Speed can be simply expressed by:

$$\omega = \frac{\Delta N}{\Sigma T_{sc,acc} + \Delta T_{h-1} - \Delta T_h} \cdot \frac{2\pi}{N_p} \quad [rad \cdot s^{-1}] \rightarrow \frac{\Delta N}{\Sigma T_{sc,acc} + \Delta T_{h-1} - \Delta T_h} \cdot \frac{60}{N_p} \quad [RPM] \tag{8}$$

where ΔN is the number of encoder pulses received within the observation (basic or extended) window.

The strength of the method can be identified inside its *iterative nature*, as a consequence of the fact that always the same kind of time interval is measured within each cycle. A very important consequence of this fact is that the same algorithm and speed calculation formula is adopted for both low- and high-speed operations, that is no commutation between different measuring algorithms is to be provided. This

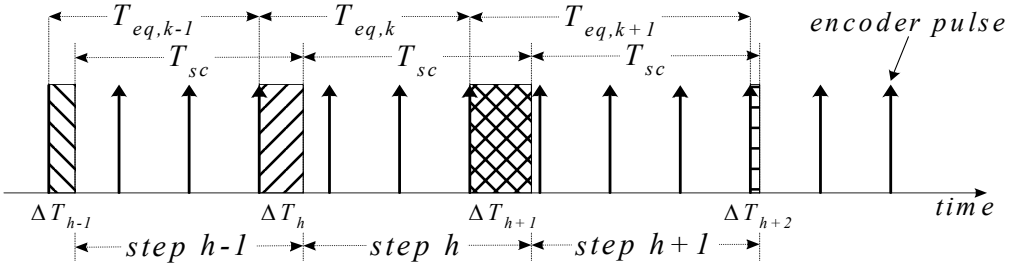

Fig. 5. Explanation of the mixed-mode frequency and period measuring method.

allows to adopt a simple hardware subsystem, normally found inside common μCs (timer plus capture unit) with no recourse to additional hardware, [11].

The accuracy of the method is limited only by the quantisation error that is inevitably introduced in time measurement performed by digital counter, whose effect on speed measurement error is almost always negligible. Then the provided accuracy is comparable to that of a pure time measurement in low speed region, extended to all the pulses received in a full speed sampling period. In the high speed region the accuracy is always higher and asymptotically reaches that of frequency measurement. In fact, after a certain (high) value of speed, the period of the high frequency counter (T_{hf}) used for time interval measurements becomes comparable to the period of the encoder signals. The corresponding quantisation error becomes then non-negligible with respect to the accuracy of pure frequency measurement. Finally, the high frequency counter resolution is to be designed based on the ratio between the speed sampling period and the timer frequency, being therefore upper limited in all the operating conditions.

The measuring error is a function of the operating conditions, in terms of speed value and synchronisation between encoder pulses, measuring window width and period of the high frequency counter. It could be demonstrated that its value is given by the following expression:

$$e_\omega\% = \frac{2 \cdot T_{hf}}{\Sigma T_{sc,acc} + \Delta T_{h-1} - \Delta T_h + 2 \cdot T_{hf}} \cdot 100 \,. \tag{9}$$

and a comparison with other solutions is also shown in Fig. 4.

The main problem to be faced in the implementation of the proposed measurement algorithm is the correct sampling of the data needed for speed calculation. At a certain time instant within each speed calculation cycle the number of acquired encoder pulses ΔN and the time interval ΔT_h have to be measured, together with the width of the observation window (T_{sc} or $\Sigma T_{sc,acc}$). The number of the encoder pulses ΔN is provided by the quadrature decode logic and the associated counter. The time interval ΔT_h is obtained through a capture unit associated with a free running timer unit. From each set of acquired data, (8) can be applied for speed calculation within that cycle.

Different cases can originate incoherence of sampled data and has to be fully identified and studied in order to compensate for them, [11].

IV. OBSERVER-BASED METHODS

Proper state models of the dynamic behaviour of mechanical subsystem (including position, speed, acceleration, etc.) can be arranged providing speed estimation in real-time based on easily measurable quantities and system parameters by means of state observers and estimators. Both determistic (Lunberger like) and non-deterministic (Kalman Filter based) will be considered here.

A. Kalman Filter

Kalman filter is an optimal recursive algorithm which provides the minimum variance state estimation for a time-varying linear system. It is able to tolerate system modelling and measurement errors, which are considered as noise processes in the state estimation. It processes all available measurements regardless of their precision, to provide a quick and accurate estimate of the variables of interest, also achieving a fast convergence. Its extension to non-linear systems, the Extended Kalman Filter (EKF), does not assure the minimum variance estimate and no convergence proof can be given. Nevertheless, the approach behaves well in most situations, as demonstrated by numerous applications.

For a straightforward application of this algorithm, the non-linear discrete-time state equations of the system are written in the following form:

$$\begin{cases} \boldsymbol{x}_{k+1} = \boldsymbol{f}(\boldsymbol{x}_k, \boldsymbol{u}_k, \mathrm{k}) + \boldsymbol{w}_k & cov(\boldsymbol{w}) = E(\boldsymbol{w}\boldsymbol{w}^T) = \boldsymbol{Q} \\ \boldsymbol{y}_k = \boldsymbol{h}(\boldsymbol{x}_k, \boldsymbol{u}_k, \mathrm{k}) + \boldsymbol{v}_k & cov(\boldsymbol{v}) = E(\boldsymbol{v}\boldsymbol{v}^T) = \boldsymbol{R} \end{cases} \tag{10}$$

where $\boldsymbol{x}_k$ is the system state vector, $\boldsymbol{y}_k$ is the system output, $\boldsymbol{u}_k$ is the system input, $\boldsymbol{w}_k$ and $\boldsymbol{v}_k$ are zero-mean white Gaussian additive noises with covariance $\boldsymbol{Q}$ and $\boldsymbol{R}$, respectively (independent from the system state $\boldsymbol{x}_k$). The vector $\boldsymbol{w}_k$ takes into account the system disturbances and model inaccuracies, while $\boldsymbol{v}_k$ represents the measurement noise. A block diagram of the EKF for the system (10) is shown in Fig. 6 and the list of the steps of a recursive implementation is provided by (11). The filter provides a first estimate of $\boldsymbol{x}$ ($\tilde{\boldsymbol{x}}$, prediction) based on the model equations and assuming that model noise is zero. Then the measurements and noise models are used to generate the sub-optimal estimate $\hat{\boldsymbol{x}}$. $\tilde{\boldsymbol{P}}$ and $\hat{\boldsymbol{P}}$ are the prediction and the estimation error covariance matrices respectively.

Speed estimation is obtained by means of a non-linear state model based on the orthogonal components (*sin-cos*) representation of a rotating space vector, whose discrete time form is considered in (12), ω_b being a proper scaling value.

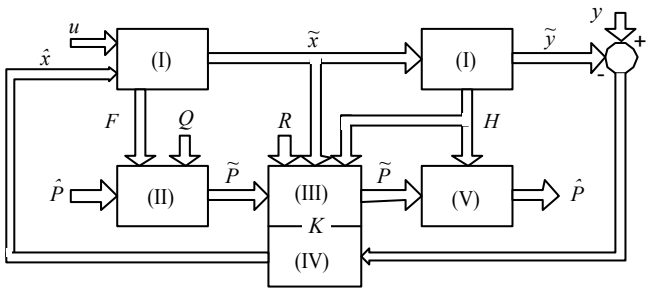

Fig. 6. EKF recursive computational block diagram.

$$\tilde{\boldsymbol{x}} = \boldsymbol{f}(\hat{\boldsymbol{x}}, \boldsymbol{u}) \qquad \tilde{\boldsymbol{y}} = \boldsymbol{h}(\tilde{\boldsymbol{x}}, \boldsymbol{u})$$

$$\text{I)} \quad \boldsymbol{F} = \left.\frac{\partial \boldsymbol{f}(\boldsymbol{x})}{\partial \boldsymbol{x}}\right|_{\boldsymbol{x}=\hat{\boldsymbol{x}}} \qquad \boldsymbol{H} = \left.\frac{\partial \boldsymbol{h}(\boldsymbol{x})}{\partial \boldsymbol{x}}\right|_{\boldsymbol{x}=\hat{\boldsymbol{x}}}$$

$$\text{II)} \quad \tilde{\boldsymbol{P}} = \boldsymbol{F}\hat{\boldsymbol{P}}\boldsymbol{F}^T + \boldsymbol{Q} \tag{11}$$

$$\text{III)} \quad \boldsymbol{K} = \tilde{\boldsymbol{P}}\,\boldsymbol{H}^T\left[\boldsymbol{H}\tilde{\boldsymbol{P}}\boldsymbol{H}^T + \boldsymbol{R}\right]^{-1}$$

$$\text{IV)} \quad \hat{\boldsymbol{x}} = \tilde{\boldsymbol{x}} + \boldsymbol{K}(\boldsymbol{y} - \tilde{\boldsymbol{y}})$$

$$\text{V)} \quad \hat{\boldsymbol{P}} = \tilde{\boldsymbol{P}} - \boldsymbol{K}\boldsymbol{H}\tilde{\boldsymbol{P}}$$

As shown in Fig. 7, the position generated from the encoder is highly affected by the quantisation noise and the filter allows to estimate both the components of the rotating space vector (*sin-cos* components) and the pulsation (ω) with an accuracy which is independent from the sensor's resolution. Moreover one sample of the estimated orthogonal components and the estimated frequency is available at each execution of the EKF, even if no encoder pulse is received in that step.

The computational requirements of the estimation algorithm are relatively high, as a number of matrix calculations has to be performed on-line at each step, and are a function of chosen numerical precision and representation of the variables. Accuracy and convergence speed of the estimates are affected by the choice of system parameters, especially the state covariance matrix $\boldsymbol{Q}$ (e.g. a high value of the parameter q speeds up the convergence but provides a high ripple of the estimates at steady state). That is the reason why adaptive solutions have been proposed by some authors in the recent past, [15].

$$\boldsymbol{x}_{k+1} = \boldsymbol{f}(\boldsymbol{x}_k, \mathrm{k}) = \begin{pmatrix} x_1 \cdot cos(\omega_b T_{sc} \cdot x_3) - x_2 \cdot sin(\omega_b T_{sc} \cdot x_3) \\ x_1 \cdot sin(\omega_b T_{sc} \cdot x_3) + x_2 \cdot cos(\omega_b T_{sc} \cdot x_3) \\ x_3 \end{pmatrix}$$

$$\boldsymbol{y}_k = \begin{pmatrix} 1 & 0 & 0 \\ 0 & 1 & 0 \end{pmatrix} \cdot \boldsymbol{x}_k = \begin{bmatrix} cos\theta_k & sin\theta_k \end{bmatrix}^T \tag{12}$$

$$\boldsymbol{x}_k = \begin{bmatrix} cos\theta_k & sen\theta_k & \omega_k \end{bmatrix}^T, \ \boldsymbol{u}_k = \begin{bmatrix} 0 & 0 \end{bmatrix}^T,$$

$$\boldsymbol{Q} = q\boldsymbol{I}_{3x3}, \ \boldsymbol{R} = r\boldsymbol{I}_{2x2}$$

An interesting alternative approach is presented in [13]. It is based on the linear state model (13) that depends only on the sampling period T and where an estimation of acceleration is also included.

$$\boldsymbol{x}_{k+1} = \boldsymbol{A} \cdot \boldsymbol{x}_k + \boldsymbol{b} \cdot \breve{a}_k + \boldsymbol{w}_k$$
$$y_k = \boldsymbol{c} \cdot \boldsymbol{x}_k + r_k$$

$$\boldsymbol{A} = \begin{bmatrix} 1 & T & \frac{T^2}{2} \\ 0 & 1 & T \\ 0 & 0 & 1 \end{bmatrix}, \ \boldsymbol{b}^T = \begin{bmatrix} \frac{T^2}{2} & T & 0 \end{bmatrix}, \ \boldsymbol{c}^T = \begin{bmatrix} 1 & 0 & 0 \end{bmatrix}. \tag{13}$$

where $\boldsymbol{x}_k = [\theta_r, \omega_r, \varepsilon_r]_k^T$ is the vector of state variables, $\boldsymbol{w}_k$ takes into account the system disturbances and model inaccuracies, $y_k = \theta_r$ is the measured variable and $\boldsymbol{r}_k$ models measuring errors (i.e. quantisation of the position signal).

A stationary Kalman filter can therefore be employed for optimal state estimation and design of the parameters of the filter can be done off-line with a classical pole allocation procedure. In this way the number of real-time operations to be performed are reduced.

B. Luenberger observer

Alternative approaches to motor speed (and position) estimation make use of closed loop observers (i.e. Luenberger observer), based on the measurement of rotor position and, if necessary, applied torque. This method enables the estimation of position too, overcoming the problems related to the adoption of low-resolution position transducers for motor drive control as estimated position is available also when no pulse is received by the encoder.

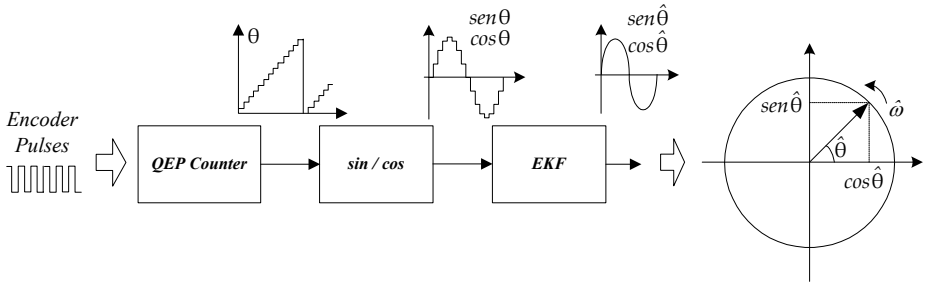

Fig. 7. Configuration for position filtering and speed estimation.

A copy of the mechanical subsystem of the drive (14) is considered, with total inertia being J_m and viscous friction B_m, that are initially considered constant and known parameters. The state form of the system is given in (15), and a standard observer is build to estimate its vector state variables, (16).

$$\tau(t) = J_m\ddot{\theta}(t) + B_m\dot{\theta}(t) \tag{14}$$

$$\begin{cases} \dot{\underline{x}}(t) = \boldsymbol{A}\underline{x}(t) + \boldsymbol{B}u(t) \\ y(t) = \boldsymbol{C}\underline{x}(t) + Du(t) \end{cases}$$

$$\boldsymbol{A} = \begin{bmatrix} 0 & 1 \\ 0 & -\frac{B_m}{J_m} \end{bmatrix},\ B = \begin{bmatrix} 0 \\ \frac{1}{J_m} \end{bmatrix},\ \boldsymbol{C} = \begin{bmatrix} 1 & 0 \end{bmatrix},\ D = 0 \tag{15}$$

$$\underline{x}(t) = \begin{bmatrix} x_1(t) \\ x_2(t) \end{bmatrix} = \begin{bmatrix} \theta(t) \\ \dot{\theta}(t) \end{bmatrix},\ u(t) = \tau(t)$$

$$\dot{\underline{\hat{x}}}(t) = \boldsymbol{A}\underline{\hat{x}}(t) + \boldsymbol{B}u(t) - \boldsymbol{LC}\left(\underline{\hat{x}}(t) - \underline{x}(t)\right),\ \boldsymbol{L} = \begin{bmatrix} l_1 \\ l_2 \end{bmatrix} \tag{16}$$

The error dynamical equation is shown in (17) where $\boldsymbol{L}$ is the observer gain matrix. Eigenvalues of the dynamical matrix $(\boldsymbol{A} - \boldsymbol{LC})$ can be easily calculated as a function of system parameters J_m and B_m, (18). Dynamics of the estimation error can therefore be imposed in the observer design phase by a proper choice of the gains l_1 and l_2.

$$\dot{\underline{e}}(t) = (\boldsymbol{A} - \boldsymbol{LC})\underline{e}(t). \tag{17}$$

$$\lambda_{1,2} = \frac{-\left(l_1 + \frac{B_m}{J_m}\right) \pm \sqrt{\left(l_1 + \frac{B_m}{J_m}\right)^2 - 4\left(l_1\frac{B_m}{J_m} + l_2\right)}}{2} \tag{18}$$

Uncertainty on the knowledge of parameters modify system matrices and therefore the values of eigenvalues. Let us consider that actual inertia and viscous friction be modeled as nominal values plus variation terms, that is:

$$J_m^* = J_m + \Delta_J,\ B_m^* = B_m + \Delta_B. \tag{19}$$

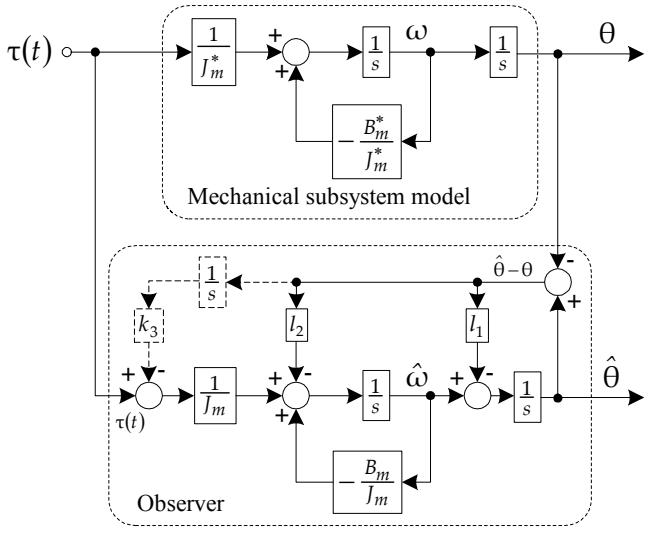

Fig. 8. Luenberger observer for position and speed estimation.

The actual mechanical system model differs from (15) as system matrices can be arranged in order to include the variation terms Δ_J and Δ_B:

$$\begin{cases} \dot{\underline{x}}(t) = \boldsymbol{A}^*\underline{x}(t) + \boldsymbol{B}^*u(t) \\ y(t) = \boldsymbol{C}\underline{x}(t) + Du(t) \end{cases}$$

$$\boldsymbol{A}^* = \begin{bmatrix} 0 & 1 \\ 0 & -\frac{B_m + \Delta_B}{J_m + \Delta_J} \end{bmatrix}^{\Delta} = \boldsymbol{A} - \delta\boldsymbol{A},\ \boldsymbol{B}^* = \begin{bmatrix} 0 \\ \frac{1}{J_m + \Delta_J} \end{bmatrix}^{\Delta} = \boldsymbol{B} - \delta\boldsymbol{B}, \tag{20}$$

$$\boldsymbol{C} = \begin{bmatrix} 1 & 0 \end{bmatrix},\ D = 0,$$

$$\delta\boldsymbol{A} = \begin{bmatrix} 0 & 0 \\ 0 & -\frac{B_m}{J_m} + \frac{B_m + \Delta_B}{J_m + \Delta_J} \end{bmatrix},\ \delta\boldsymbol{B} = \begin{bmatrix} 0 \\ \frac{1}{J_m} - \frac{1}{J_m + \Delta_J} \end{bmatrix}$$

Fig. 8 resumes the block diagram of the mechanical subsystem and the corresponding observer models. Contribution of the dashed terms will be considered in the following. Calculation of the observer estimation error dynamics from (16) and (20) leads to the following expression, taking into account variation of the system parameters through matrices $\delta\boldsymbol{A}$ and $\delta\boldsymbol{B}$:

$$\dot{\underline{e}}(t) = (\boldsymbol{A} - \boldsymbol{LC})\underline{e}(t) + \delta\boldsymbol{A}\underline{x}(t) + \delta\boldsymbol{B}u(t), \tag{21}$$

the corresponding solution in time domain being

$$\underline{e}(t) = \left[s\boldsymbol{I} - (\boldsymbol{A} - \boldsymbol{LC})\right]^{-1} \bullet \\ \bullet \left\{\delta\boldsymbol{A}\left[s\boldsymbol{I} - (\boldsymbol{A} - \delta\boldsymbol{A})\right]^{-1}(\boldsymbol{B} - \delta\boldsymbol{B}) + \delta\boldsymbol{B}\right\}u(t). \tag{22}$$

It can be proved that steady-state response of the error vector, that is position and speed estimation errors, to a step change in the system input $u(t)$ is not zero, thus limiting the adoption of the considered observer to actual drive system where mechanical parameters are not exactly identified or can vary during system operations. Fig. 9 shows the simulation results of the observer when only a variation of viscous friction is considered. Position and speed estimation errors are clearly visible during input torque steady-state conditions.

Rejection to step change in system input is obtained by an additional fictitious state variable added to the system (15) as proposed by [2]. An additive integral term of position estimation error is added to the input torque aiming at compensating errors in

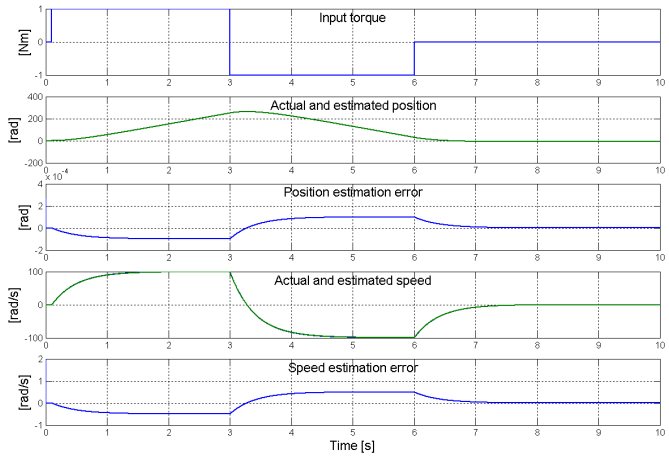

Fig. 9. Simulation results for Luenberger observer with no integral correction.

speed and position estimation (dashed blocks in Fig. 8). The dynamical system used for estimation can be modified as follows:

$$\begin{cases} \dot{\underline{x}}_{ext}(t) = \boldsymbol{A}^*_{ext}\,\underline{x}_{ext}(t) + \boldsymbol{B}^*_{ext}u(t) \\ y(t) = \boldsymbol{C}_{ext}\,\underline{x}_{ext}(t) + Du(t) \end{cases}$$

$$\boldsymbol{A}^*_{ext} = \begin{bmatrix} 0 & 1 & 0 \\ 0 & -\frac{B_m+\Delta_B}{J_m+\Delta_J} & 0 \\ 0 & 0 & 0 \end{bmatrix} \overset{\Delta}{=} \boldsymbol{A}_{ext} - \delta\boldsymbol{A}_{ext},$$

$$\boldsymbol{B}^*_{ext} = \begin{bmatrix} 0 \\ \frac{1}{J_m+\Delta_J} \\ 0 \end{bmatrix} \overset{\Delta}{=} \boldsymbol{B}_{ext} - \delta\boldsymbol{B}_{ext}, \qquad (23)$$

$$\boldsymbol{C}_{ext} = \begin{bmatrix} 1 & 0 & 0 \end{bmatrix},\ D = 0,\ \boldsymbol{L}_{ext} = \begin{bmatrix} l_1 \\ l_2 \\ 1 \end{bmatrix}$$

$$\delta\boldsymbol{A}_{ext} = \begin{bmatrix} 0 & 0 & 0 \\ 0 & -\frac{B_m}{J_m} + \frac{B_m+\Delta_B}{J_m+\Delta_J} & \frac{k_3}{J_m} \\ 0 & 0 & 0 \end{bmatrix},\ \delta\boldsymbol{B}_{ext} = \begin{bmatrix} 0 \\ \frac{1}{J_m} - \frac{1}{J_m+\Delta_J} \\ 0 \end{bmatrix}$$

where k_3 is an additional gain affecting the integration velocity of the position estimation error and has to be chosen in the design phase together with parameters l_1 and l_2 of the standard observer. Analytical results can be provided by considering the same expressions (21) and (22), proving that steady-state response of the error vector to a step change in the system input $u(t)$ is zero both for position and speed, as shown in Fig. 10 where the same overall conditions of Fig. 9 are considered.

Accuracy of the method is limited only by the numerical precision of the calculations and the implementation efforts are very light when compared to other observers (e.g. Kalman filter). When compared to other observer-based methods, common problems of the choice of the gains arise. Traditional design procedures can be successfully adopted in continuous time domain. But time domain discretisation and the quantisation noise of the measured position signal affects and limits the performance of the method and the overall accuracy and noise of the estimates. Moreover input torque knowledge is not always trivial to obtain with the necessary accuracy.

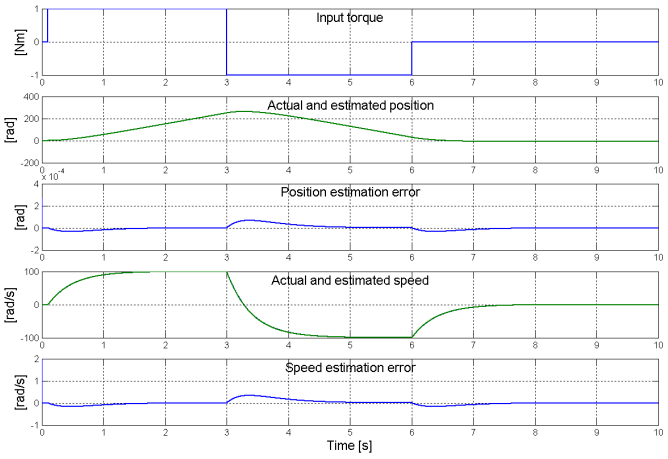

Fig. 10. Simulation results for Luenberger observer with integral correction.

V. Conclusions

In this paper a comparative analysis of state-of-art speed measurement and estimation algorithms suitable for low-resolution incremental encoder equipped drives has been presented. The specific feature of each one has been analysed, both from the performance point of view (i.e. accuracy and dynamic response) and from the computational requirements needed for the actual implementation.

References

[1] R.M. Kennel, "Why do incremental encoders do a reasonable good job in electrical drives with digital control," *Proceedings of the 41st IEEE Industry Applications Society Annual Meeting,* Tampa, FL, USA, Volume 2, pp. 925÷930, 8÷12 October, 2006.

[2] R.D. Lorenz, K.W. Van Pattern, "High-Resolution Velocity Estimation for All-Digital ac Servo Drives," *IEEE Transactions on Industry Applications*, Vol. 27, No. 4, July/August 1991.

[3] F. Briz, J. A. Cancelas, A. Diez, "Speed Measurement Using Rotary Encoders for High Performance AC Drives," *Proceedings of the 20th International Conference on Control and Instrumentation (IECON '94)*, vol. 1, Page 538÷542, 5÷9 September, 1994.

[4] B.J. Brunsbach, G. Henneberger, Th. Klepsch, "Speed Estimation with Digital Position Sensor," *Proceedings of the International Conference on Electrical Machines (ICEM'92)*, pp. 577÷581, Manchester, 1992.

[5] G. Liu, "On Velocity Estimation Using Position Measurements," *Proceedings of the American Control Conference*, Anchorage, AK, May 8÷10, 2002.

[6] R. Fararooy, "Accurate and Fast Speed Measurement Using Ramp-Waveform Sampling Technique," *Letters of the IEEE Transactions on Industrial Electronics*, Vol. 46, No. 5, October 1999.

[7] M. Prokin, "Extremely Wide-Range Speed Measurement Using a Double-Buffer Method," *IEEE Transactions on Industrial Electronics*, vol. 41, No. 5, October 1994.

[8] N. Stojkovic, Z. Stare, N. Mijat, "Dual-Mode Digital Revolution Counter," *Proceedings of the 18th IEEE Instrumentation and Measurement Technology Conference (IMTC'01)*, Vol. 2, Page 950÷954, 21÷23 May, 2001.

[9] N. Ekekwe, R. Etienne-Cummings , P. Kazanzides, "Incremental Encoder Based Position and Velocity Measurements VLSI Chip with Serial Peripheral Interface," *Proceedings of the IEEE International Symposium on Circuits and Systems (ISCAS'2007)*, New Orleans, LA, USA, pp. 3558÷3561, 27-30 May, 2007.

[10] R.C. Kavanagh, "Improved Digital Tachometer With Reduced Sensitivity to Sensor Nonideality," *IEEE Transactions on Industrial Electronics*, Vol. 47, No. 4, August 2000.

[11] R. Petrella, M. Tursini, "An Embedded System for Position and Speed Measurement Adopting Incremental Encoders," *IEEE Transactions on Industry Applications*, in press.

[12] M. Labbate, R. Petrella, M. Tursini, "Fixed point implementation of Kalman filtering for AC drives: a case study using TMS320F24x DSP," *Proceedings of the 3rd European DSP Education and Research Conference*, Paris, France, September 20÷21, 2000.

[13] A. Bellini, S. Bifaretti, S. Costantini, "Identification of the mechanical parameters in high-performance drives," *Proceeding of the European Power Electronics Conference (EPE'2001)*, Graz, 2001.

[14] H. Kin, S. Yi, N. Kim, R.D. Lorenz, "Using Low Resolution Position Sensors in Bumpless Position/Speed Estimation Methods for Low Cost PMSM Drives," *Proceedings of the 40th IEEE Industry Applications Society Annual Meeting*, Hong Kong, 2005.

[15] D. Luong-Van, M.J. Tordon, J.Katupitiya, "Covariance Profiling for an Adaptive Kalman Filter to Suppress Sensor Quantization Effects," *Proceedings of the 43rd IEEE Conference on Decision and Control*, Atlantis, Paradise Island, Bahamas, December 14-17, 2004.